J. Fluid Mech. (2005), *vol.* 542, *pp.* 69–96. © 2005 Cambridge University Press
doi:10.1017/S0022112005005185 Printed in the United Kingdom

An asymptotic description of vortex Kelvin modes

By STÉPHANE LE DIZÈS AND LAURENT LACAZE

Institut de Recherche sur les Phénomènes Hors Équilibre, 49, rue F. Joliot-Curie, BP 146, F-13384 Marseille cedex 13, France

(Received 17 November 2003 and in revised form 14 February 2005)

A large-axial-wavenumber asymptotic analysis of inviscid normal modes in an axisymmetric vortex with a weak axial flow is performed in this work. Using a WKBJ approach, general conditions for the existence of regular neutral modes are obtained. Dispersion relations are derived for neutral modes confined in the vortex core ('core modes') or in a ring ('ring modes'). Results are applied to a vortex with Gaussian vorticity and axial velocity profiles, and a good agreement with numerical results is observed for almost all values of k. The theory is also extended to deal with singular modes possessing a critical point singularity. We demonstrate that the characteristics for vanishing viscosity of viscous damped normal modes can also be obtained. Known viscous damped eigenfrequencies for the Gaussian vortex without axial flow are, in particular, shown to be predicted well by our estimates. The theory is also shown to provide explanations for a few of their peculiar properties.

1. Introduction

Kelvin modes are the inviscid normal modes which are associated with the rotation of the fluid in a stable vortex. They often describe the possible small deformations of the vortex. They are also known to be resonantly excited in various situations (elliptic instability; precessional instability; parametric forcing). The goal of this work is to construct an asymptotic theory which provides the spatial structure and the dispersion relation of these modes.

The simplest Kelvin modes are for an infinite uniform solid-body rotation. In that case, there exist plane wave solutions in the rotating frame (the so-called Kelvin waves) which can be summed to form a localized inviscid normal mode (Greenspan 1968). If the solid-body rotation is within an infinite cylinder, the frequency ω of the modes is discretized for any fixed axial wavenumber k and azimuthal wavenumber m and satisfies a dispersion relation. Moreover, in that case, Kelvin modes form a basis, so all the deformations can be expressed in terms of Kelvin modes. If the solid-body rotation is surrounded by an irrotational fluid (Rankine vortex), the Kelvin modes satisfy similar properties (e.g. Saffman 1992). They also form a basis for the perturbations confined within the vortex core (Arendt, Fritts & Andreassen 1997).

Kelvin modes are also known to exist, when the vorticity field is not constant. Some of their properties were analysed for a Gaussian vortex without axial flow in Fabre (2002), Sipp & Jacquin (2003) and Fabre, Sipp & Jacquin (2005). Sipp & Jacquin (2003) used an inviscid approach. They showed that regular inviscid normal modes

exist in a frequency interval similar to that obtained for the Rankine vortex; however, to the interval where ω/m is in the range of the angular velocity, has to be excluded. In that frequency interval, regular inviscid normal modes do not exist anymore: they possess a critical point singularity. If this singularity is smoothed by viscosity, these modes apparently become damped with a damping rate which is largely independent of viscosity (if sufficiently small) as shown by Fabre (2002) and Fabre *et al.* (2005). An inviscid estimate of this damping rate can be obtained by avoiding the singularity in the complex plane as was done by Sipp & Jacquin (2003). Such a procedure has been justified in Le Dizès (2004) where the viscous critical layer has been resolved. In the present work, we implicitly assume a viscous problem with vanishing viscosity. This implies that, for a few modes, the path of integration of the inviscid equation has to be deformed in the complex plane, for the equation to remain asymptotically valid. In practice, this means that the critical point singularities have to be avoided in the complex plane, following the classical rule used for two-dimensional modes in planar flows (see Lin 1955).

When an axial flow is present, regular inviscid neutral modes are still expected to exist, however, very little information on their properties is available in the literature. Moreover, axial flow may promote instability in a stable vortex. For instance, the Batchelor vortex, which is a vortex with Gaussian vorticity and axial velocity profiles, is known to possess unstable inviscid modes if the axial flow is sufficiently large (see, for instance Ash & Khorrami 1995). Here, our interest is not in these modes. Instead, we shall focus on vortices which are stable in a non-viscous framework. Our goal is to provide some information on the neutral and damped modes of such vortices in a general setting using an asymptotic approach.

The approach is based on a large-axial-wavenumber asymptotic analysis. In this limit, the radial structure of the normal modes varies on a faster scale than the characteristic radial scale of the base flow. These fast variations can be captured by a WKBJ theory (see for instance Bender & Orszag 1978) and are shown to depend in a simple way on the base flow characteristics. For neutral modes, they are also shown to be either pure oscillations or pure exponentials, with the transition between the two types of behaviour occurring at the turning points where WKBJ approximations break down. As with the original quantum mechanics framework, eigenmodes are constructed by forming solutions which are localized in the oscillatory regions; the dispersion relation being nothing but a discretization of the number of oscillations.

In the present work, two types of modes are considered: modes confined between the vortex centre and a turning point ('core modes') and modes confined between two distant turning points ('ring modes'). The paper is organized as follows. In § 2, base flow and perturbation equations are presented. Section 3 is devoted to the large-wavenumber asymptotic analysis in a general setting. Conditions for the existence of regular neutral modes in the WKBJ framework are derived. The spatial structure and the dispersion relation of core modes and ring modes are then obtained. The results are applied to a Gaussian vortex with or without axial velocity in § 4. The case without axial flow is considered first in § 4.1. In this section, the results for core modes are also extended to deal with a critical layer singularity. Both singular neutral core modes and damped core modes are obtained and compared to numerical results. In § 4.2, the asymptotic results are applied to the Gaussian vortex with axial flow (Batchelor vortex). The last section summarizes the main results and discusses a possible application of the results to the elliptic instability.

2. Basic flow and perturbation equations

Consider a general axisymmetric vortex with axial flow, whose velocity field may be written in cylindrical coordinates in the form:

$$\boldsymbol{U}_b(r) = (0, V(r), W(r)). \tag{2.1}$$

This vortex has an angular velocity $\Omega(r)$ and an axial vorticity $\zeta(r)$ given by:

$$\Omega(r) = \frac{V(r)}{r}, \tag{2.2a}$$

$$\zeta(r) = \frac{1}{r}\frac{\mathrm{d}(rV)}{\mathrm{d}r}. \tag{2.2b}$$

In this study, viscous diffusion is not taken into account with the implicit assumption that the Reynolds number is sufficiently large. The base flow, defined by (2.1), satisfies the incompressible Euler equations regardless of the profile V and W, as long as it represents a regular field in cylindrical coordinates (in particular $V(0)=0$). The asymptotic analysis detailed in the next section will be carried out for arbitrary profiles. However, in the applications, we shall only consider Gaussian vorticity and axial velocity profiles. Time and spatial scales are non-dimensionalized by the angular velocity in the vortex centre, and the core size, respectively; such that $\Omega(r)$ and $W(r)$ read:

$$\Omega(r) = \frac{1-\mathrm{e}^{-r^2}}{r^2}, \tag{2.3a}$$

$$W(r) = W_0\,\mathrm{e}^{-r^2}, \tag{2.3b}$$

where W_0 is a constant measuring the strength of the axial flow.

We shall be concerned with inviscid linear perturbations in the form of normal modes:

$$(\boldsymbol{U}, P) = (u, v, w, p)\mathrm{e}^{\mathrm{i}kz+\mathrm{i}m\theta-\mathrm{i}\omega t}, \tag{2.4}$$

where k and m are axial and azimuthal wavenumbers and ω is the frequency. The equations for the velocity and pressure amplitudes (u, v, w, p) are:

$$\mathrm{i}\Phi u - 2\Omega v = -\frac{\mathrm{d}p}{\mathrm{d}r}, \tag{2.5a}$$

$$\mathrm{i}\Phi v + \zeta u = -\frac{\mathrm{i}mp}{r}, \tag{2.5b}$$

$$\mathrm{i}\Phi w + W'w = -\mathrm{i}kp, \tag{2.5c}$$

$$\frac{1}{r}\frac{\mathrm{d}(ru)}{\mathrm{d}r} + \frac{\mathrm{i}mv}{r} + \mathrm{i}kw = 0, \tag{2.5d}$$

where a prime denotes a derivative with respect to r, and

$$\Phi(r) = -\omega + m\Omega(r) + kW(r). \tag{2.6}$$

Equations (2.5a)–(2.5d) can be reduced to a single equation for the pressure p (see Saffman 1992; Le Dizès 2004) to form:

$$\frac{\mathrm{d}^2p}{\mathrm{d}r^2} + \left(\frac{1}{r} - \frac{\Delta'}{\Delta}\right)\frac{\mathrm{d}p}{\mathrm{d}r} + \left(\frac{2m}{r\Phi\Delta}(\Omega'\Delta - \Omega\Delta') + \frac{k^2\Delta}{\Phi^2} - \frac{m^2}{r^2} - \frac{2mkW'\Omega}{r\Phi^2}\right)p = 0, \tag{2.7}$$

where

$$\Delta(r) = 2\zeta(r)\Omega(r) - \Phi^2(r). \tag{2.8}$$

If Δ and Φ do not vanish at zero, the condition that p remains bounded at ∞ and at $r=0$ transforms (2.7) into an eigenvalue problem for ω (assuming k and m are fixed). The case where $\Phi(0)$ is close to zero will not be considered here. It requires a specific study by itself. We refer to Fabre (2002) for the Gaussian vortex without axial flow. Partial results for the Batchelor vortex can also be found in Stewartson & Leibovich (1987) and Stewartson & Brown (1985).

The objective of this work is to provide information on the dispersion relation and on the spatial structure of the eigenmode. Our approach is based on an asymptotic analysis for large k.

3. Large k asymptotic analysis

In this section, the asymptotic analysis is presented in a general framework. Applications are considered in the next section.

The principle of the analysis is to construct approximate solutions valid in the limit $k\to\infty$. For large k, when there is no axial flow, or if the axial flow scales as $1/k$, the expression before p in (2.7) becomes particularly simple as it reduces to a single term $k^2\Delta/\Phi^2$. Therefore, for large k, this term has to be equilibrated by rapid variation of the pressure amplitude on the scale rk. Such variations can be captured by a WKBJ analysis (see Bender & Orszag 1978). In this framework, the perturbation pressure is expanded as

$$p=\left(p_0(r)+\frac{p_1(r)}{k}+\cdots\right)\mathrm{e}^{k\phi(r)}. \tag{3.1}$$

The expression for $\phi(r)$ is obtained at order k^2:

$$\left(\frac{\mathrm{d}\phi}{\mathrm{d}r}\right)^2=-\frac{\Delta}{\Phi^2}, \tag{3.2}$$

where we have assumed in the expression (2.6) for Φ that the axial flow is small and can be written as

$$kW\equiv W_1=O(1). \tag{3.3}$$

From (3.2), it follows that:

$$\phi(r)=\pm\mathrm{i}\int^r\frac{\sqrt{\Delta}}{\Phi}\,\mathrm{d}r. \tag{3.4}$$

At order k, an equation for $p_0(r)$ is obtained:

$$2\phi'\frac{\mathrm{d}p_0}{\mathrm{d}r}+\left[\phi'\left(\frac{1}{r}-\frac{\Delta'}{\Delta}\right)+\phi''\right]p_0=0, \tag{3.5}$$

which gives, for both functions ϕ,

$$p_0(r)=\sqrt{\frac{\Phi}{r}}\Delta^{1/4}. \tag{3.6}$$

Expressions (3.1), (3.4) and (3.6) provide two independent leading-order approximations of solutions to (2.7). These so-called WKBJ approximations break down at the vortex centre $r=0$, and at the points where Φ or Δ vanishes. The vortex centre is a regular singularity which comes from the use of cylindrical coordinates. As shown below, this singularity can be easily smoothed by carrying out a local analysis for $r=O(1/k)$. Points where $\Delta=0$ are the so-called turning points of the WKBJ approximations. In the neighbourhood of these turning points, the two approximations

are no longer independent. We can also show that higher-order corrections, such as p_1 in the expansion (3.1), diverge at turning points. These turning-point singularities can also be resolved by a local analysis of the turning-point region (Bender & Orszag 1978, see also below). Finally, the singularities where $\Phi = 0$, i.e. $\omega = m\Omega + W_1$, are the so-called critical points of the inviscid approximation. As our choice is to stay inviscid, we shall not resolve these singularities here. Instead, if such a singularity appears, it will be avoided by deforming the integration space of (2.7) in the complex r-plane, in order to stay in the regions of the complex plane where the inviscid approximation remains valid (Sipp & Jacquin 2003; Le Dizès 2004). In those cases, the inviscid solutions would become singular in the physical domain.

If we restrict for a moment our attention to regular neutral eigenmodes, a few results can be obtained in a general setting. By definition, for those modes, both the frequency ω and the wavenumber k are real and $\Phi(r)$ never vanishes on the real axis. The WKBJ approximations constructed for the present problem are then very similar to those initially introduced by Wentzel, Kramers and Brillouin for describing the bounded states of a particle in a potential well in quantum mechanics (see Landau & Lifchitz 1966). If $\Delta > 0$, WKBJ approximations are oscillating functions, if $\Delta < 0$, they are exponentials. In the semi-classical description of quantum mechanics, this corresponds to oscillating wave functions in regions where the energy level is larger than the local potential and evanescent exponentials where it is smaller. As in that framework where it is proved that there is no energy level smaller than the potential minimum, we can prove here that there does not exist a regular neutral eigenmode for which Δ remains negative for all r. Indeed if $\Delta < 0$ for all r, both WKBJ approximations are uniformly valid in any interval of $]0, +\infty[$, and no combination of these approximations can be matched to solutions which are bounded at the origin and at infinity (see also below). The conclusion is, therefore, that Δ must be non-negative somewhere for a regular neutral mode to exist. To analyse this condition of existence, it is useful to define what is often called the epicyclic frequencies $\omega^{\pm}(r)$ of the vortex at the radial coordinate r:

$$\omega^{\pm} = m\Omega(r) + W_1(r) \pm \sqrt{2\Omega(r)\zeta(r)}. \tag{3.7}$$

In this expression, the quantity $\Upsilon(r) = 2\Omega(r)\zeta(r)$ is what is called the Rayleigh discriminant. It characterizes the unstable character of the vortex with respect to the centrifugal instability (see Drazin & Reid 1981). In the stable vortex that we consider, Υ is always non-negative which implies that ω^+ and ω^- are real functions. These two functions provide the frequency interval where Δ is positive, that is $\Delta(r) > 0$ if and only if $\omega^-(r) < \omega < \omega^+(r)$. It is also useful to consider the function

$$\omega_c(r) = m\Omega(r) + W_1(r), \tag{3.8}$$

which provides the (critical) frequency of the mode that exhibits a critical point at the radial location r. We can now easily deduce the frequency intervals where regular neutral modes can exist. Their frequency must be somewhere between ω^- and ω^+ without being in the range of ω_c. The regular neutral mode frequencies then satisfy

$$\min(\omega^-) \leqslant \omega \leqslant \min(\omega_c), \tag{3.9}$$

or

$$\max(\omega_c) \leqslant \omega \leqslant \max(\omega^+). \tag{3.10}$$

Moreover, the upper bound in (3.9) and the lower bound in (3.10) can be excluded if the extrema are reached for finite r.

In the quantum mechanics framework, bounded states are known to be discretized by their number of oscillations in the potential well (see Landau & Lifchitz 1966). We shall see below that the same result is obtained here: eigenmodes will be localized in the region where $\Delta > 0$ and selected by a discretization condition on their number of oscillations in that region. In the rest of this section, we shall obtain this discretization condition when there is a single interval of positive Δ. More precisely, we shall assume that the functions Δ and Φ satisfy one of the two hypotheses:

HYPOTHESIS H1. *The function Δ is positive for $0 \leqslant r < r_t$, negative for $r > r_t$ and has a single zero r_t. The function Φ does not vanish on the real axis.*

HYPOTHESIS H2. *The function Δ is positive for $r_1 < r < r_2$, negative for $0 \leqslant r < r_1$ and $r_2 < r$, and has two simpl zeros r_1 and r_2. The function Φ does not vanish on the real axis.*

When Hypothesis H1 is satisfied, eigenmodes are localized between 0 and r_t. We shall denote such modes as 'core modes'. When Hypothesis H2 is satisfied, eigenmodes are localized between r_1 and r_2 and for this reason are termed 'ring modes'. For the vortices considered in § 4, regular neutral modes will be found to be either core modes or ring modes. However, for vortices with a more complex profile, we could imagine more complex modes, corresponding to configurations with multiple distinct regions where Δ is positive. Each type of mode would require a specific analysis, but it can follow the approach which is now presented for 'core modes' and 'ring modes'.

In § 4, it will also be shown how the above hypotheses can be extended to deal with complex frequencies.

3.1. *Core modes*

When Hypothesis H1 is satisfied, the mode structure can be decomposed into four regions.

(i) The neighbourhood of the centre $r = 0$.
(ii) The 'core' region between 0 and r_t.
(iii) The neighbourhood of the turning point r_t.
(iv) The 'outer' region for $r > r_t$.

In each region, a specific approximation of the mode is obtained. The condition of matching of the different approximations will provide the dispersion relation.

The neighbourhood of $r = 0$

In order to smooth the singularity of the WKBJ approximations at $r = 0$, we introduce the local variable $\bar{r} = kr$ and expand the perturbation pressure as

$$\bar{p}(\bar{r}) = \bar{p}_0(\bar{r}) + \frac{\bar{p}_1(\bar{r})}{k} + \cdots. \tag{3.11}$$

At leading order, $\bar{p}_0$ is found to satisfy:

$$\frac{\mathrm{d}^2\bar{p}_0}{\mathrm{d}\bar{r}} + \frac{1}{\bar{r}}\frac{\mathrm{d}\bar{p}_0}{\mathrm{d}\bar{r}} + \left(\frac{\Delta(0)}{\Phi^2(0)} - \frac{m^2}{\bar{r}^2}\right)\bar{p}_0 = 0. \tag{3.12}$$

The solution which is bounded at $\bar{r} = 0$ is given by:

$$\bar{p}_0 = a_0 J_{|m|}(\beta_0 \bar{r}), \tag{3.13}$$

where a_0 is a constant, $J_{|m|}$ is the usual Bessel function of the first kind and β_0 is a positive constant given by:

$$\beta_0 = \frac{\sqrt{\Delta(0)}}{\Phi(0)}. \tag{3.14}$$

The 'core' region $(0 < r < r_t)$

In the 'core' region, the WKBJ approximations are valid and are oscillating functions. The matching with the solution valid in the neighbourhood of $r = 0$ provides a condition on the solution in this region.

The function $J_m(z)$ in (3.13) has the following expansion (see Abramowitz & Stegun 1965) for large $|z|$:

$$J_{|m|}(z) \sim \sqrt{\frac{2}{\pi z}} \cos\left(z - \tfrac{1}{2}|m|\pi - \tfrac{1}{2}\pi\right), \quad |\arg(z)| < \pi. \tag{3.15}$$

This guarantees that the leading-order expression (3.13) can match (as $\bar{r} \to \infty$) a combination of WKBJ approximations:

$$p \sim A^+ p_0(r)\, \mathrm{e}^{k\phi} + A^- p_0(r)\, \mathrm{e}^{-k\phi}, \tag{3.16}$$

provided that,

$$A^+ \mathrm{e}^{k\phi(0)} = \frac{a_0}{\sqrt{2\pi\Delta(0)k}}\, \mathrm{e}^{-\mathrm{i}|m|\pi/2 - \mathrm{i}\pi/4}, \tag{3.17a}$$

$$A^- \mathrm{e}^{-k\phi(0)} = \frac{a_0}{\sqrt{2\pi\Delta(0)k}}\, \mathrm{e}^{\mathrm{i}|m|\pi/2 + \mathrm{i}\pi/4}, \tag{3.17b}$$

that is,

$$A^\pm = A_0\, \mathrm{e}^{\mp k\phi(0)} \exp\left(\mp \tfrac{1}{2}\mathrm{i}|m|\pi \mp \tfrac{1}{4}\mathrm{i}\pi\right). \tag{3.18}$$

It follows that a leading-order approximation for the solution in this region is given by

$$p \sim A_0 \sqrt{\frac{\Phi}{r}}\, \Delta^{1/4} \cos\left(k \int_0^r \frac{\sqrt{\Delta}}{\Phi}\, \mathrm{d}r - \tfrac{1}{2}|m|\pi - \tfrac{1}{4}\pi\right), \tag{3.19}$$

where A_0 is a constant which can be expressed in terms of a_0.

The 'outer' region $(r > r_t)$

In the 'outer' region, one of the WKBJ approximations is exponentially increasing while the other is exponentially decreasing. In order to form a solution which vanishes for large r, the exponentially growing WKBJ approximation should not be present in the solution. It follows that for $r > r_t$, the solution can be written at leading order as:

$$p \sim B_0 \sqrt{\frac{\Phi}{r}}(-\Delta)^{1/4} \exp\left(-k \int_{r_t}^r \frac{\sqrt{-\Delta}}{\Phi}\, \mathrm{d}r\right). \tag{3.20}$$

The matching of the 'outer' region with the 'core' region is performed in the neighbourhood of the turning point r_t. This provides the dispersion relation and a relation between the coefficients A_0 and B_0 of (3.19) and (3.20).

Neighbourhood of the turning point r_t

The local analysis of the neighbourhood of a simple turning point is classical (see for instance Bender & Orszag 1978). Following the textbooks, we introduce a local

variable $\tilde{r} = (r - r_t)k^{2/3}$, where the power 2/3 is typical of a simple turning-point analysis, and expands the perturbation pressure as:

$$\tilde{p}(\tilde{r}) = \tilde{p}_0(\tilde{r}) + k^{-1/3}\tilde{p}_1(\tilde{r}) + \cdots. \tag{3.21}$$

At leading order, an equation is obtained for $\tilde{p}_0$:

$$\frac{\mathrm{d}^2\tilde{p}_0}{\mathrm{d}\tilde{r}^2} - \frac{1}{\tilde{r}}\frac{\mathrm{d}\tilde{p}_0}{\mathrm{d}\tilde{r}} + \frac{\Delta_t'\tilde{r}}{\Phi_t^2}\tilde{p}_0 = 0. \tag{3.22}$$

This equation can be integrated as:

$$\tilde{p}_0(\tilde{r}) = b_0\mathrm{Ai}'(\kappa\tilde{r}) + c_0\mathrm{Bi}'(\kappa\tilde{r}), \tag{3.23}$$

where b_0 and c_0 are constants, $\mathrm{Ai}(z)$ and $\mathrm{Bi}(z)$ are Airy functions (see Abramowitz & Stegun 1965) and $\kappa = (-\Delta_t'/\Phi_t^2)^{1/3}$.

Dispersion relation

The matching of the 'turning-point region' with the 'outer' region requires that the exponentially growing function Bi' in (3.23) should not be present in the solution, that is $c_0 = 0$. Using the following expansions (Abramowitz & Stegun 1965) of $\mathrm{Ai}'(z)$ for large $|z|$:

$$\mathrm{Ai}'(z) \sim -\frac{1}{2\sqrt{\pi}}z^{1/4}\exp\left(-\tfrac{2}{3}z^{3/2}\right), \quad |\arg(z)| < \pi, \tag{3.24a}$$

$$\mathrm{Ai}'(-z) \sim -\frac{1}{\sqrt{\pi}}z^{1/4}\cos\left(\tfrac{2}{3}z^{3/2} + \tfrac{1}{4}\pi\right), \quad |\arg(z)| < \tfrac{2}{3}\pi, \tag{3.24b}$$

we obtain the relation:

$$-\frac{b_0}{2\sqrt{\pi}}\kappa^{1/4}k^{1/6} = B_0\sqrt{\frac{\Phi_t}{r_t}}(-\Delta_t')^{1/4}, \tag{3.25}$$

from the matching with the 'outer' region, and

$$-\frac{b_0}{\sqrt{\pi}}\kappa^{1/4}k^{1/6}\,\mathrm{e}^{-\mathrm{i}\pi/4} = A_0\sqrt{\frac{\Phi_t}{r_t}}(-\Delta_t')^{1/4}\exp\left(\mathrm{i}k\int_0^{r_t}\frac{\sqrt{\Delta}}{\Phi}\,\mathrm{d}r - \tfrac{1}{2}\mathrm{i}|m|\pi - \tfrac{1}{4}\mathrm{i}\pi\right), \tag{3.26a}$$

$$-\frac{b_0}{\sqrt{\pi}}\kappa^{1/4}k^{1/6}\,\mathrm{e}^{\mathrm{i}\pi/4} = A_0\sqrt{\frac{\Phi_t}{r_t}}(-\Delta_t')^{1/4}\exp\left(-\mathrm{i}k\int_0^{r_t}\frac{\sqrt{\Delta}}{\Phi}\,\mathrm{d}r + \tfrac{1}{2}\mathrm{i}|m|\pi + \tfrac{1}{4}\mathrm{i}\pi\right), \tag{3.26b}$$

from the matching with the 'core' region. Equations (3.25) and (3.26) yield

$$A_0^2 = 4B_0^2 \tag{3.27}$$

and the dispersion relation that links k, m and ω:

$$\exp\left(2\mathrm{i}k\int_0^{r_t}\frac{\sqrt{\Delta}}{\Phi}\,\mathrm{d}r - \mathrm{i}|m|\pi\right) = 1, \tag{3.28}$$

which can also be written as:

$$k = \frac{|m|\pi + 2n\pi}{2\displaystyle\int_0^{r_t}\sqrt{\Delta}/\Phi}\,\mathrm{d}r, \quad \text{where } n \text{ is a non-negative integer.} \tag{3.29}$$

We recall that in the above expression, Φ and Δ are given by (2.6) and (2.8) respectively, and that r_t is a zero of Δ. Expression (3.29) is the dispersion relation for 'core' modes in the limit of large k.

Spatial structure of the eigenmodes

Approximations for the pressure perturbation can now be obtained in each region using (3.25) and (3.27). They depend on a unique amplitude factor A_0 which can be fixed to 1 such that a_0, B_0 and b_0 are now given by

$$a_0 = \sqrt{\tfrac{1}{2}\pi\Delta_0 k}, \tag{3.30a}$$

$$B_0 = \tfrac{1}{2}(-1)^n, \tag{3.30b}$$

$$b_0 = -k^{-1/6}(-1)^n\sqrt{\frac{\pi}{r_t}}\Phi_t^{2/3}(-\Delta_t')^{1/6}. \tag{3.30c}$$

Approximations for the velocity field are also easily derived from p using (2.5) which gives

$$u = -\frac{\mathrm{i}\Phi}{\Delta}\frac{\mathrm{d}p}{\mathrm{d}r} - \frac{2\mathrm{i}m\Omega}{r\Delta}p, \tag{3.31a}$$

$$v = \frac{\zeta}{\Delta}\frac{\mathrm{d}p}{\mathrm{d}r} + \frac{m\Phi}{r\Delta}p, \tag{3.31b}$$

$$w = -\frac{k}{\Phi}p. \tag{3.31c}$$

We obtain the following expressions.
In the 'core' region:

$$p \sim \sqrt{\frac{\Phi}{r}}\Delta^{1/4}\cos\left(k\int_0^r \frac{\sqrt{\Delta}}{\Phi}\,\mathrm{d}r - \tfrac{1}{2}|m|\pi - \tfrac{1}{4}\pi\right), \tag{3.32a}$$

$$u \sim \mathrm{i}k\sqrt{\frac{\Phi}{r}}\Delta^{-1/4}\sin\left(k\int_0^r \frac{\sqrt{\Delta}}{\Phi}\,\mathrm{d}r - \tfrac{1}{2}|m|\pi - \tfrac{1}{4}\pi\right), \tag{3.32b}$$

$$v \sim -\frac{k\zeta\Delta^{-1/4}}{\sqrt{r\Phi}}\sin\left(k\int_0^r \frac{\sqrt{\Delta}}{\Phi}\,\mathrm{d}r - \tfrac{1}{2}|m|\pi - \tfrac{1}{4}\pi\right), \tag{3.32c}$$

$$w \sim -\frac{k\Delta^{1/4}}{\sqrt{r\Phi}}\cos\left(k\int_0^r \frac{\sqrt{\Delta}}{\Phi}\,\mathrm{d}r - \tfrac{1}{2}|m|\pi - \tfrac{1}{4}\pi\right). \tag{3.32d}$$

In the neighbourhood of r_t ($r - r_t = O(k^{-2/3})$):

$$p \sim -k^{-1/6}(-1)^n\sqrt{\frac{\pi}{r_t}}\Phi_t^{2/3}(-\Delta_t')^{1/6}\mathrm{Ai}'\big(\kappa(r-r_t)k^{2/3}\big), \tag{3.33a}$$

$$u \sim -\mathrm{i}k^{7/6}(-1)^n\sqrt{\frac{\pi}{r_t}}\Phi_t^{1/3}(-\Delta_t')^{-1/6}\mathrm{Ai}\big(\kappa(r-r_t)k^{2/3}\big), \tag{3.33b}$$

$$v \sim k^{7/6}(-1)^n\sqrt{\frac{\pi}{r_t}}\Phi_t^{-2/3}(-\Delta_t')^{-1/6}\zeta_t\mathrm{Ai}\big(\kappa(r-r_t)k^{2/3}\big), \tag{3.33c}$$

$$w \sim k^{5/6}(-1)^n\sqrt{\frac{\pi}{r_t}}\Phi_t^{-1/3}(-\Delta_t')^{1/6}\mathrm{Ai}'\big(\kappa(r-r_t)k^{2/3}\big), \tag{3.33d}$$

with $\kappa = (-\Delta_t'/\Phi_t^2)^{1/3}$.

Near the origin $r = O(1/k)$:

$$p \sim \sqrt{\frac{\pi\Delta_0 k}{2}} J_{|m|}(\beta_0 kr), \tag{3.34a}$$

$$u \sim -\mathrm{i}\sqrt{\frac{\pi}{2}} k^{3/2} \left(J'_{|m|}(\beta_0 kr) + \frac{2m\Omega_0}{\sqrt{\Delta_0} kr} J_{|m|}(\beta_0 kr) \right), \tag{3.34b}$$

$$v \sim \sqrt{\frac{\pi}{2}} k^{3/2} \left(\frac{\zeta_0}{\Phi_0} J'_{|m|}(\beta_0 kr) - \frac{m\Phi_0}{\sqrt{\Delta_0} kr} J_{|m|}(\beta_0 kr) \right), \tag{3.34c}$$

$$w \sim -\sqrt{\frac{\pi\Delta_0}{2\Phi_0^2}} k^{3/2} J_{|m|}(\beta_0 kr), \tag{3.34d}$$

with $\beta_0 = \sqrt{\Delta_0}/\Phi_0$.
In the 'outer' region:

$$p \sim \tfrac{1}{2}(-1)^n \sqrt{\frac{\Phi}{r}} (-\Delta)^{1/4} \exp\left(-k \int_{r_t}^{r} \frac{\sqrt{-\Delta}}{\Phi} \, \mathrm{d}r \right), \tag{3.35a}$$

$$u \sim -\mathrm{i}k \tfrac{1}{2}(-1)^n \sqrt{\frac{\Phi}{r}} (-\Delta)^{-1/4} \exp\left(-k \int_{r_t}^{r} \frac{\sqrt{-\Delta}}{\Phi} \, \mathrm{d}r \right), \tag{3.35b}$$

$$v \sim \tfrac{1}{2}(-1)^n \frac{k(-\Delta)^{-1/4}}{\sqrt{r\Phi}} \exp\left(-k \int_{r_t}^{r} \frac{\sqrt{-\Delta}}{\Phi} \, \mathrm{d}r \right), \tag{3.35c}$$

$$w \sim -\tfrac{1}{2}(-1)^n \frac{k(-\Delta)^{1/4}}{\sqrt{r\Phi}} \exp\left(-k \int_{r_t}^{r} \frac{\sqrt{-\Delta}}{\Phi} \, \mathrm{d}r \right). \tag{3.35d}$$

These expressions will be compared to numerical results in the applications considered in § 4.

3.2. *Ring modes*

When Hypothesis H2 is satisfied, the eigenmode structure can be divided into the following regions:

(i) The neighbourhood of the origin.
(ii) The 'outer' region I for $0 < r < r_1$.
(iii) The neighbourhood of the turning point r_1.
(iv) The 'ring' region for $r_1 < r < r_2$.
(v) The neighbourhood of the turning point r_2.
(vi) The 'outer' region II for $r > r_2$.

The analysis is very similar to that performed for 'core modes'. In the neighbourhood of the origin, the pressure is expressed in terms of Bessel functions. A leading-order approximation is given by (3.13), but β_0 is now purely imaginary. Near the origin, the pressure can be written as:

$$\bar{p}_0 = a_0 I_{|m|}(\gamma_0 \bar{r}), \tag{3.36}$$

where a_0 is a constant, $I_{|m|}$ is the usual Bessel function of second kind and,

$$\gamma_0 = \frac{\sqrt{-\Delta(0)}}{\Phi(0)}. \tag{3.37}$$

For large $\bar{r}$, (3.36) becomes exponentially large. In the outer region I, the solution can therefore be approximated by a single WKBJ wave:

$$p \sim A_I \sqrt{\frac{\Phi}{r}} (-\Delta)^{1/4} \exp\left(k \int_0^r \frac{\sqrt{-\Delta}}{\Phi} \, \mathrm{d}r \right), \tag{3.38}$$

where the matching imposes a relation between A_I and a_0. Note that if Δ was negative everywhere, the outer region would extend up to infinity, and the approximation (3.38) would be unbounded for large r, invalidating the boundary condition at $+\infty$. This justifies the condition of existence stated above which requires a region of positive Δ.

In the outer region II, the solution is, as above, given by the subdominant WKBJ approximation:

$$p \sim A_{II} \sqrt{\frac{\Phi}{r}} (-\Delta)^{1/4} \exp\left(-k \int_{r_2}^r \frac{\sqrt{-\Delta}}{\Phi} \, \mathrm{d}r \right). \tag{3.39}$$

The solution in the turning point region near r_2 which matches this expression is, as above:

$$p \sim a_2 \mathrm{Ai}'(\kappa_2 \check{r}), \tag{3.40}$$

where $\check{r} = (r - r_2)k^{2/3}$ and $\kappa = (-\Delta_2'/\Phi_2^2)^{1/3}$.

Similarly, the solution in the turning point region near r_1 which matches expression (3.38) is:

$$p \sim a_1 \mathrm{Ai}'(\kappa_1 \tilde{r}), \tag{3.41}$$

where $\tilde{r} = (r - r_1)k^{2/3}$ and $\kappa = -(\Delta_1'/\Phi_1^2)^{1/3}$.

Expressions (3.41) and (3.40) imply that in the 'ring' region, the solution admits approximations of the form:

$$p \sim A_0 \sqrt{\frac{\Phi}{r}} \Delta^{1/4} \cos\left(k \int_{r_1}^r \frac{\sqrt{\Delta}}{\Phi} \, \mathrm{d}r + \tfrac{1}{4}\pi \right), \tag{3.42}$$

and

$$p \sim B_0 \sqrt{\frac{\Phi}{r}} \Delta^{1/4} \cos\left(k \int_{r_2}^r \frac{\sqrt{\Delta}}{\Phi} \, \mathrm{d}r - \tfrac{1}{4}\pi \right), \tag{3.43}$$

where A_0 and B_0 can be expressed in terms of a_1 and a_2, respectively. These two expressions are compatible only if

$$\sin\left(k \int_{r_1}^{r_2} \frac{\sqrt{\Delta}}{\Phi} \, \mathrm{d}r + \tfrac{1}{2}\pi \right) = 0,$$

that is,

$$k = \frac{n\pi + \pi/2}{\displaystyle\int_{r_1}^{r_2} \frac{\sqrt{\Delta}}{\Phi}}, \quad \text{where } n \text{ is a non-negative integer.} \tag{3.44}$$

Expression (3.44) is the dispersion relation for 'ring modes' in the limit of large k.

Spatial structure of the eigenmodes

As for the core modes, approximations for the pressure and the velocity field of ring modes can now easily be obtained in each region. If we fix $A_0 = 1$, we obtain in each region the following expressions.

In the 'ring' region

$$p \sim \sqrt{\frac{\Phi}{r}}\Delta^{1/4}\cos\left(k\int_{r_1}^{r}\frac{\sqrt{\Delta}}{\Phi}\,\mathrm{d}r+\tfrac{1}{4}\pi\right), \tag{3.45a}$$

$$u \sim \mathrm{i}k\sqrt{\frac{\Phi}{r}}\Delta^{-1/4}\sin\left(k\int_{r_1}^{r}\frac{\sqrt{\Delta}}{\Phi}\,\mathrm{d}r+\tfrac{1}{4}\pi\right), \tag{3.45b}$$

$$v \sim -\frac{k\zeta\Delta^{-1/4}}{\sqrt{r\Phi}}\sin\left(k\int_{r_1}^{r}\frac{\sqrt{\Delta}}{\Phi}\,\mathrm{d}r+\tfrac{1}{4}\pi\right), \tag{3.45c}$$

$$w \sim -\frac{k\Delta^{1/4}}{\sqrt{r\Phi}}\cos\left(k\int_{r_1}^{r}\frac{\sqrt{\Delta}}{\Phi}\,\mathrm{d}r+\tfrac{1}{4}\pi\right). \tag{3.45d}$$

In the region near the turning point r_1, defined by $r-r_1=O(k^{-2/3})$:

$$p \sim k^{-1/6}\sqrt{\pi}\Phi_1^{2/3}r_1^{-1/2}(\Delta_1')^{1/6}\mathrm{Ai}'\big(\kappa_1(r-r_1)k^{2/3}\big), \tag{3.46a}$$

$$u \sim -ik^{7/6}\sqrt{\pi}\Phi_1^{1/3}r_1^{-1/2}(\Delta_1')^{-1/6}\mathrm{Ai}\big(\kappa_1(r-r_1)k^{2/3}\big), \tag{3.46b}$$

$$v \sim k^{7/6}\sqrt{\pi}\Phi_1^{-2/3}r_1^{-1/2}(\Delta_1')^{-1/6}\zeta_1\mathrm{Ai}\big(\kappa_1(r-r_1)k^{2/3}\big), \tag{3.46c}$$

$$w \sim -k^{5/6}\sqrt{\pi}\Phi_1^{-1/3}r_1^{-1/2}(\Delta_1')^{1/6}\mathrm{Ai}'\big(\kappa_1(r-r_1)k^{2/3}\big), \tag{3.46d}$$

with $\kappa_1=(\Delta_1'/\Phi_1^2)^{1/3}$.

In the region near the turning point r_2, defined by $r-r_2=O(k^{-2/3})$:

$$p \sim -k^{-1/6}(-1)^n\sqrt{\pi}\Phi_2^{2/3}r_2^{-1/2}(-\Delta_2')^{1/6}\mathrm{Ai}'\big(\kappa_2(r-r_2)k^{2/3}\big), \tag{3.47a}$$

$$u \sim -\mathrm{i}k^{7/6}(-1)^n\sqrt{\pi}\Phi_2^{1/3}r_2^{-1/2}(-\Delta_2')^{-1/6}\mathrm{Ai}\big(\kappa_2(r-r_2)k^{2/3}\big), \tag{3.47b}$$

$$v \sim k^{7/6}(-1)^n\sqrt{\pi}\Phi_2^{-2/3}r_2^{-1/2}(-\Delta_2')^{-1/6}\zeta_2\mathrm{Ai}\big(\kappa_2(r-r_2)k^{2/3}\big), \tag{3.47c}$$

$$w \sim k^{5/6}(-1)^n\sqrt{\pi}\Phi_2^{-1/3}r_2^{-1/2}(-\Delta_2')^{1/6}\mathrm{Ai}'\big(\kappa_2(r-r_2)k^{2/3}\big), \tag{3.47d}$$

with $\kappa_2=(-\Delta_2'/\Phi_2^2)^{1/3}$.

In the 'outer' region I:

$$p \sim \sqrt{\frac{\Phi}{4r}}(-\Delta)^{1/4}\exp\left(k\int_{r_1}^{r}\frac{\sqrt{-\Delta}}{\Phi}\,\mathrm{d}r\right), \tag{3.48a}$$

$$u \sim \mathrm{i}k\sqrt{\frac{\Phi}{4r}}(-\Delta)^{-1/4}\exp\left(k\int_{r_1}^{r}\frac{\sqrt{-\Delta}}{\Phi}\,\mathrm{d}r\right), \tag{3.48b}$$

$$v \sim -\frac{k(-\Delta)^{-1/4}}{2\sqrt{r\Phi}}\exp\left(k\int_{r_1}^{r}\frac{\sqrt{-\Delta}}{\Phi}\,\mathrm{d}r\right), \tag{3.48c}$$

$$w \sim -\frac{k(-\Delta)^{1/4}}{2\sqrt{r\Phi}}\exp\left(k\int_{r_1}^{r}\frac{\sqrt{-\Delta}}{\Phi}\,\mathrm{d}r\right), \tag{3.48d}$$

In the 'outer' region II:

$$p \sim \tfrac{1}{2}(-1)^n\sqrt{\frac{\Phi}{r}}(-\Delta)^{1/4}\exp\left(-k\int_{r_2}^{r}\frac{\sqrt{-\Delta}}{\Phi}\,\mathrm{d}r\right), \tag{3.49a}$$

$$u \sim -\mathrm{i}k\tfrac{1}{2}(-1)^n\sqrt{\frac{\Phi}{r}}(-\Delta)^{-1/4}\exp\left(-k\int_{r_2}^{r}\frac{\sqrt{-\Delta}}{\Phi}\,\mathrm{d}r\right), \tag{3.49b}$$

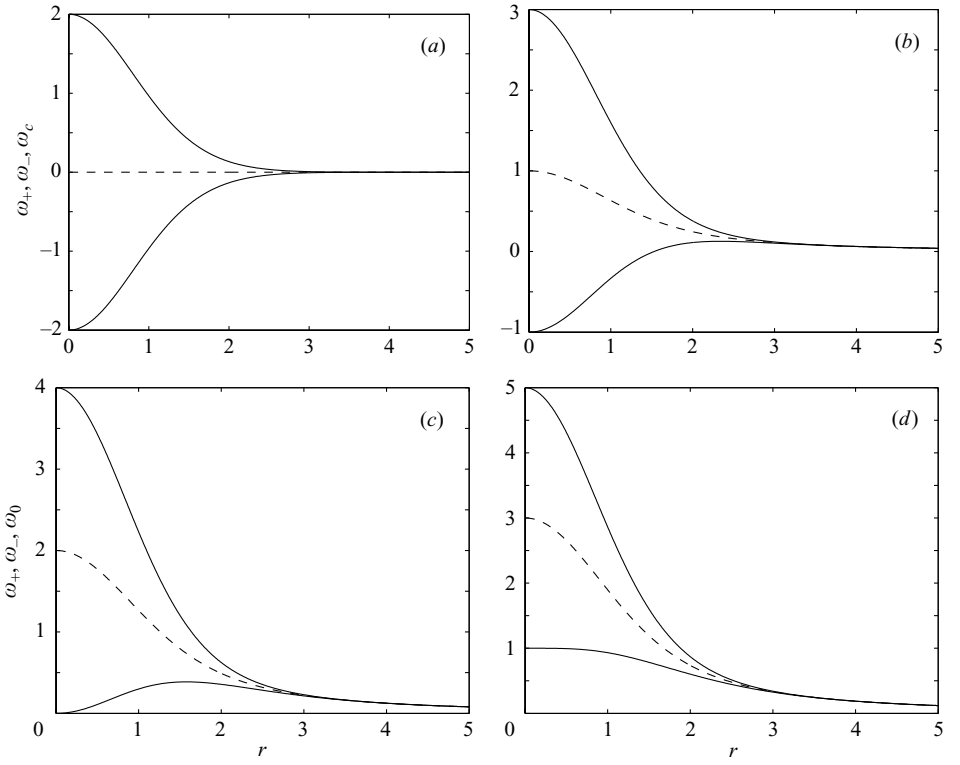

FIGURE 1. The functions $\omega^{\pm}$ (solid lines) and ω_c (dashed line) versus r for the Lamb vortex. (*a*) $m=0$; (*b*) $m=1$; (*c*) $m=2$; (*d*) $m=3$.

$$v \sim \tfrac{1}{2}(-1)^n \frac{k(-\Delta)^{-1/4}}{\sqrt{r\Phi}} \exp\left(-k\int_{r_2}^{r} \frac{\sqrt{-\Delta}}{\Phi}\,\mathrm{d}r\right), \tag{3.49c}$$

$$w \sim -\tfrac{1}{2}(-1)^n \frac{k(-\Delta)^{1/4}}{\sqrt{r\Phi}} \exp\left(-k\int_{r_2}^{r} \frac{\sqrt{-\Delta}}{\Phi}\,\mathrm{d}r\right). \tag{3.49d}$$

The above approximations for ring modes will be compared to numerical solutions in § 4.2.

4. Applications

4.1. *The Gaussian vortex without axial flow (Lamb vortex)*

In this section, we consider a Gaussian vortex without axial flow. The base flow profile is given by (2.3) with $W_0=0$. In this case, the functions $\omega^{\pm}$ and ω_c have a limited number of possible behaviours. In figure 1 the functions $\omega^{\pm}$ and ω_c are plotted for $m=0, 1, 2, 3$. For larger values of m ($m>3$), results are similar to figure 1(*d*): the three functions ω^+, ω^- and ω_c are monotonically decreasing to zero; their values at $r=0$ are $\omega^+(0)=m+2$, $\omega^-(0)=m-2$ and $\omega_c(0)=m$. The functions $\omega^{\pm}$ and ω_c, for negative m, are obtained by making the transformations $m\to -m$ and $\omega\to -\omega$.

4.1.1. *Regular neutral core modes*

The conditions (3.9) and (3.10) for the existence of regular neutral modes give here $-2\leqslant\omega\leqslant 2$ for $m=0$, $-1\leqslant\omega\leqslant 0$ and $1<\omega\leqslant 3$ for $m=1$, and $m<\omega\leqslant m+2$ for

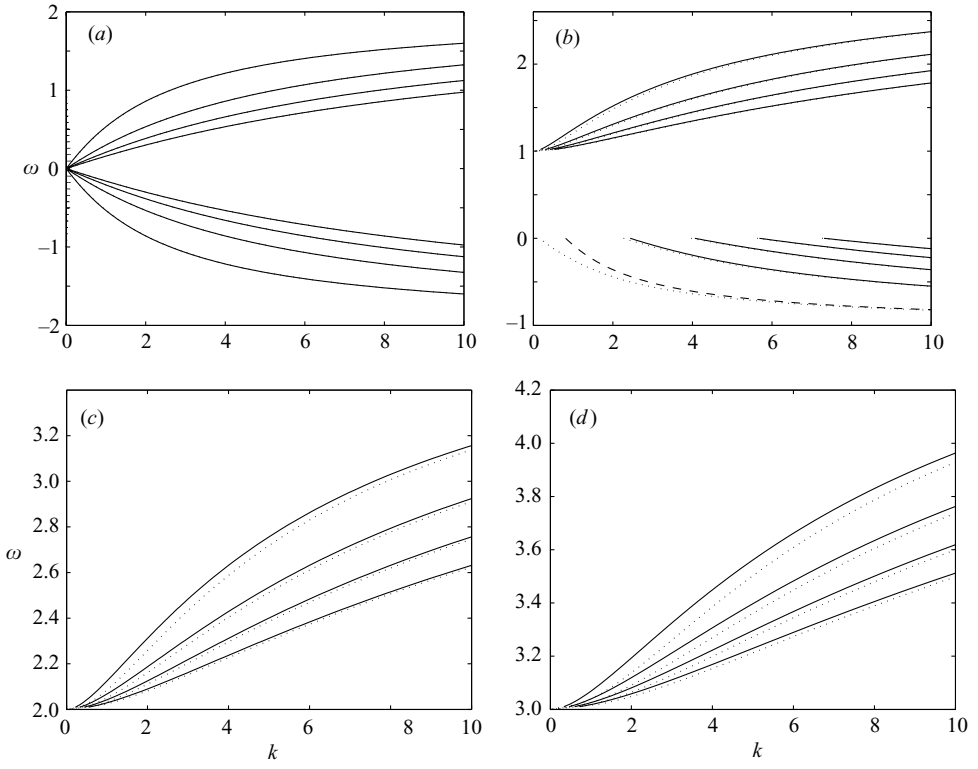

FIGURE 2. Dispersion relation of neutral core modes of the Lamb vortex. Numerical results (dotted lines) and large-k asymptotic results (expression (3.29) for $n=1, 2, 3, 4$) (solid lines). (a) $m=0$; (b) $m=1$; (c) $m=2$. (d) $m=3$. The dashed line in (b) is expression (3.29) with $n=0$.

$m \geqslant 2$. Inspection of figure 1a–d shows that in all these frequency intervals, Hypothesis H1 is satisfied. We therefore expect all regular neutral modes of the Lamb vortex to be core modes. In these frequency intervals, (3.29) can be applied. The results are displayed in solid lines in figure 2 for the first branches ($n=1, 2, 3, 4$). Dotted lines represent the dispersion relation obtained by a numerical integration of (2.7). These figures demonstrate the good agreement of the large-k dispersion relation with the numerics for not only large k, but also for small values of k. The asymptotic results also tend to be better for small m. For $m=0$, the asymptotic predictions are almost identical to the numerical results for all values of k.

For $m=1$, note that there is an additional branch for $\omega<0$ in the numerics. This branch turns out to be associated with the $n=0$ mode in (3.29). For large k, a good agreement is indeed obtained as demonstrated in figure 2(b). It is worth mentioning that the $n=0$ mode does not exist for $\omega>1$.

For all $m \geqslant 1$, the branches associated with frequencies in the interval $m<\omega \leqslant m+2$ (that is, all the branches if $m \geqslant 2$) satisfy the same property. Their frequency starts from $\omega=m$ at $k=0$, and grows monotonically with k, to $\omega=m+2$. The vanishing of k as $\omega \to m^+$ is due to the displacement of a critical point toward the origin which makes the integral in expression (3.29) divergent.

As explained above, the results for negative m are obtained by making the transformations $m \to -m$ and $\omega \to -\omega$.

4.1.2. *Singular neutral core modes*

For $m=1$, the neutral branches, obtained in the previous section, stop abruptly when ω reaches 0. For small positive frequencies, a critical point singularity r_c is now present and Δ changes sign near this point (as seen in figure 1*b*). This invalidates Hypothesis H1. If we wanted to stay on the real axis, near such a critical point, viscous effects would have to be reintroduced to smooth the singularity. As mentioned above, the inviscid equation can, however, remain valid if we avoid the critical point in the complex plane following the rule of contour deformation prescribed by Lin (1955). This rule, which can be justified in the present context by using the results of Le Dizès (2004), states that the side where the contour is deformed, is obtained by considering the displacement of the critical point for weakly amplified frequencies: if the critical point goes in the lower quadrants ($\mathrm{Im}(r_c)<0$), we have to deform the contour above the critical point, if it goes in the upper quadrants, we have to deform the contour below. In the following, this rule is systematically applied. The displacement of the critical points is monitored and it is always checked that the integration contour remains in the region of the complex plane, where the inviscid equation is asymptotically valid. It is worth mentioning that by this procedure, the inviscid limit of a viscous eigenvalue is obtained, but the corresponding eigenmode is no longer regular on the real axis. On the real axis, the eigenmode is expected to exhibit viscous oscillations which are not described by the present framework (see Fabre *et al.* 2005).

The deformation of the contour in the complex plane also implies constraints on the large k analysis. Indeed, if the critical point shifts into the complex-r plane, the validity of the WKBJ approximations in the complex plane has to be considered. In principle, this requires the analysis of the characteristic curves associated with the WKBJ approximations defined as $\mathrm{Re}(\phi)=\mathrm{Constant}$ and $\mathrm{Im}(\phi)=\mathrm{Constant}$. Among these curves, Stokes lines and Anti-Stokes lines are known to play a particular role (Olver 1997; Fedoryuk 1993); they are defined, respectively, by:

$$\mathrm{Re}\int_{r_t}^{r}\frac{\sqrt{-\Delta}}{\Phi}\,\mathrm{d}r=0, \tag{4.1}$$

and

$$\mathrm{Im}\int_{r_t}^{r}\frac{\sqrt{-\Delta}}{\Phi}\,\mathrm{d}r=0, \tag{4.2}$$

where r_t is any turning point. In the present work, we mostly use the following result which can be deduced from theorem 11.1 of Olver (1997): The WKBJ approximations are uniformly valid on any sufficiently regular finite path along which ϕ and p_0 are holomorphic and $\mathrm{Re}(\phi)$ is monotonic. Using Olver's terminology, we shall designate such a path as a progressive path. Note in particular that a part of a Stokes line which does not contain turning points and critical points is a progressive path. In this section and in the following section, our objective is to demonstrate that the asymptotic analysis of § 3.1 also applies to complex-plane configurations. The main argument of the analysis is based on the fact that the matching procedure may be performed by the same method provided that we remain on progressive paths. This guarantees that the WKBJ approximations remain uniformly valid in each region. The boundary conditions at infinity and at the origin are then transmitted up to the turning point region without modification. For the core modes, the matching at r_c can then be performed in a similar way and it leads to the same dispersion relation.

For small positive values of ω, the Stokes line structure around the real axis has the typical form displayed in figure 3. The critical point indicated by a star is close to

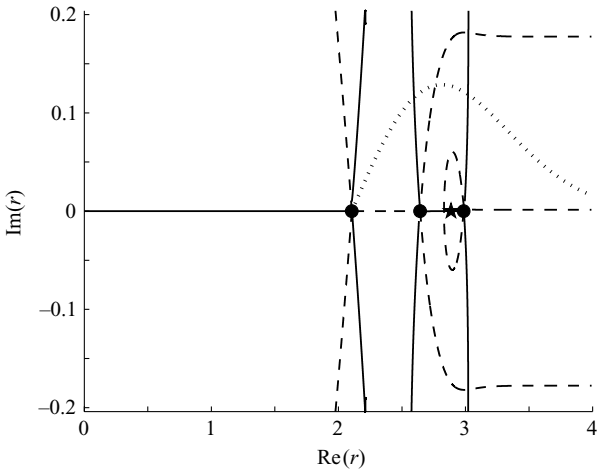

FIGURE 3. Stokes lines (solid lines) and anti-Stokes lines (dashed lines) in the complex r plane for the Lamb vortex and $\omega = 0.12$ and $m = 1$. Black circles are turning points, the star is a critical point. The dotted curve represents a progressive path along which the integration can be carried out.

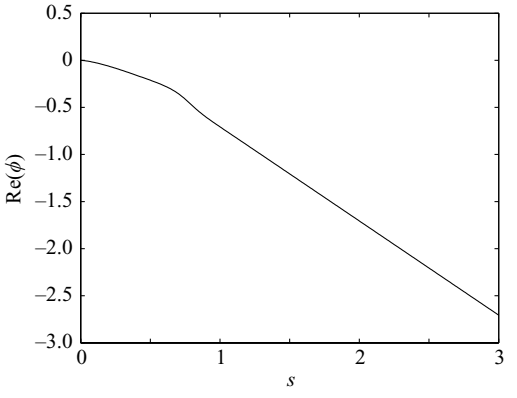

FIGURE 4. Evolution of the function $\mathrm{Re}(\phi) = \mathrm{Re}(\int_{r_t}^{r(s)} \sqrt{\Delta}/\Phi \, \mathrm{d}r)$ along the path $s \to r(s)$ indicated by a dotted line in figure 3.

two additional turning points indicated by black circles. What is remarkable is that we can find a progressive path which connects the first turning point to infinity by avoiding the critical point and the two nearby turning points in a complex region where the inviscid equation is expected to remain valid. The progressive character of the path is shown by checking that $\mathrm{Re}(\phi)$, where ϕ is given by (3.4), is a monotonic function along the path. This check has been performed and the results are shown in figure 4 for the path indicated by a dotted line in figure 3.

As WKBJ approximations are uniformly valid along this progressive path, it can replace the 'real outer region' which was considered in the previous section. The core region is as previously the interval $]0, r_t[$. As this interval is along a Stokes line, it is also a progressive path. Finally, the matching conditions across r_t can now be applied as in § 3.1, if the progressive path associated with the outer region reaches r_t on the opposite side of r_t with respect to the core region. This condition can be expressed in term of Stokes lines: the 'outer' progressive path must be in the (Stokes) sector

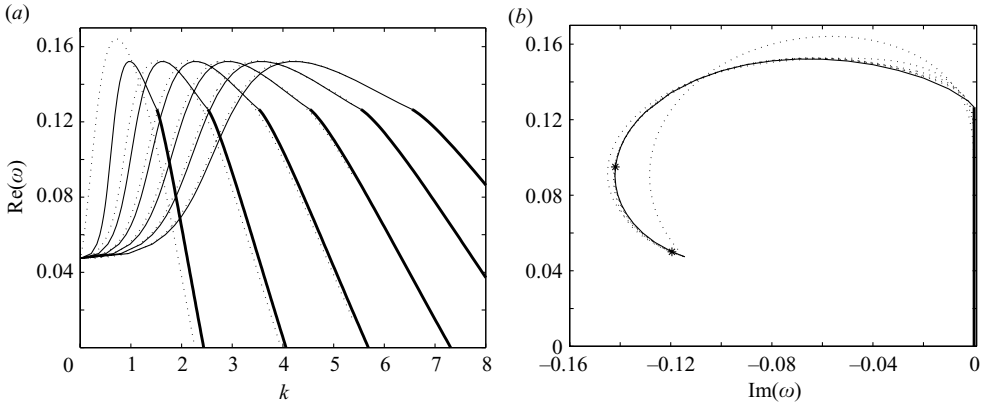

FIGURE 5. Dispersion relation of singular core modes of the Lamb vortex for $m = 1$. (a) Re(ω) versus k. (b) Re(ω) versus Im(ω). The thick solid lines indicate the neutral modes obtained in §4.1.2. The dotted lines are inviscid numerical results by Sipp & Jacquin (2003). The Stokes line structures of the eigenfrequencies indicated by stars in (b) are displayed in figure 6.

delimited by the two other Stokes lines issued from r_t (i.e. different from the Stokes line associated with the core region). The matching leads to the dispersion relation (3.29) where r_t is the first (smallest) turning point.

The typical structure (shown in figure 3), which leads to this result, is obtained in the following cases:

$$m = 1\colon 0 < \omega < \omega_c^{(1)} \approx 0.1267,$$
$$m = 2\colon 0 < \omega < \omega_c^{(2)} \approx 0.3871.$$

The critical frequencies $\omega_c^{(1)}$ and $\omega_c^{(2)}$ are the frequencies for which the first and second turning points collide for $m = 1$ and $m = 2$, respectively. These frequencies are also visible in figures 1(b) and 1(c), they correspond to the maximum values of $\omega^-(r)$.

If we apply relation (3.29) in these frequency intervals, we obtain the branches which are plotted in thick solid lines in figure 5(a) for $m = 1$ and in figure 7(a) for $m = 2$. As will be discussed in more detail below, the agreement with numerical results (dotted lines) is very good. However, it is noteworthy that the numerical frequencies possess a small negative imaginary part when the first and second turning points are close to each other. This is visible in figure 5(b) for $m = 1$ close to $\mathrm{Re}(\omega) \approx 0.12$, and in figure 7($b$) for $m = 2$ close to $\mathrm{Re}(\omega) \approx 0.35$. We think that this damping effect could be associated with higher-order corrections in $1/k$ in the asymptotic analysis.

The singular neutral modes described here do not exist for $m \geqslant 3$ when no axial flow is present. We shall see below, however, that they can appear for other values of m when an axial flow is added.

4.1.3. *Singular damped core modes*

In this section, we demonstrate that (3.29) can also be applied to obtain the inviscid limit of damped viscous eigenfrequencies. The principle has been explained above. It is to replace the real intervals by complex progressive paths. The core region between 0 and r_t is now a complex progressive path along which the two WKBJ approximations are oscillatory. This means that the core region is along a Stokes line connecting r_t to the vortex centre. The turning-point region is in the complex plane, and the outer region is a complex progressive path that goes from r_t to $+\infty$ (infinity on the real axis) and which leaves r_t on the opposite side of the core region, as explained above.

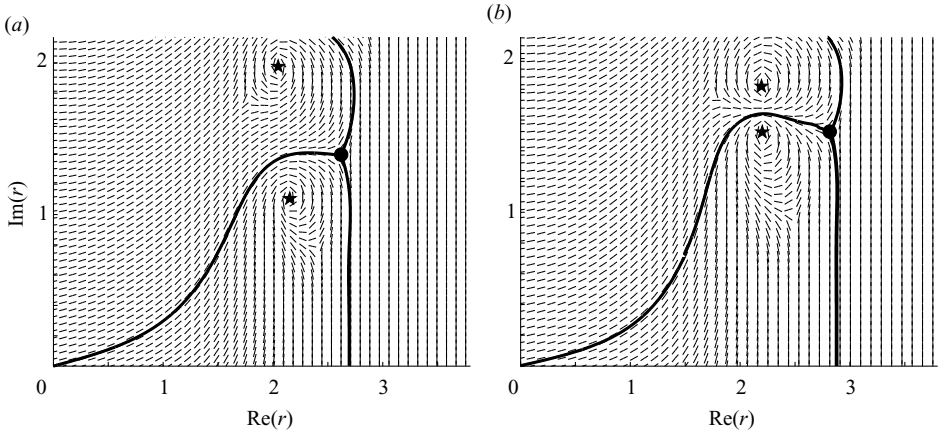

FIGURE 6. Stokes line networks for $m=1$ modes of the Lamb vortex. (a) $\omega=0.095-0.142\mathrm{i}$; ($b$) $\omega=0.05-0.119\mathrm{i}$. Stars are critical points and black circles are turning points. The relevant Stokes line network is indicated by a thick solid line. Short lines indicate on a grid the direction of the characteristic curves $\mathrm{Re}(\phi)=\mathrm{Constant}$.

In addition, the whole path that goes from 0 to ∞ (Stokes line between 0 and r_t and progressive path between r_t and $+\infty$) must avoid the critical point singularity as prescribed by Lin's rule. Checking these conditions requires a fine analysis of the Stoke line network and a monitoring of the evolution of turning points and critical points as the parameters are varied. Indeed, there are several turning points in the complex plane, so we must check that an appropriate choice is made in (3.29). Note that by contrast with the neutral modes, the integral in (3.29) has to be calculated in the complex plane, as r_t is now a complex number.

The procedure provides an asymptotic expression (for large k) for viscous damped eigenfrequencies as viscosity goes to zero. However, it is worth mentioning that the method does not provide the spatial structure of the eigenmodes on the real axis. The damped modes obtained by the contour deformation procedure are indeed expected to be singular on the real axis as the integration contour is separated from the real axis by a critical point. In fact, it is known that the true viscous damped modes exhibit viscous oscillations in an interval of the real axis (see Fabre *et al.* 2005), which cannot be described by our inviscid approach.

Examples of Stokes line structures obtained for damped eigenfrequencies are shown in figure 6 for $m=1$. The results for this value of m are shown in figure 5. Figure 5(a) displays the real part of the frequency versus k for the first four branches. Figure 5(b) shows $\mathrm{Re}(\omega)$ versus $\mathrm{Im}(\omega)$. Formula (3.29) tells us that, for all the branches, the frequencies should be on the same curve. This curve is given by the vanishing of the imaginary part in (3.29), i.e.

$$\mathrm{Im}\left(\int_0^{r_t}\frac{\sqrt{\Delta}}{\Phi}\,\mathrm{d}r\right)=0. \tag{4.3}$$

This condition is the condition mentioned above, that is one of the Stokes lines leaving the turning point r_t should pass through the origin.

In figure 5, the numerical results obtained by Sipp & Jacquin (2003) by a non-viscous shooting method with contour deformation are shown in dotted lines. As can be seen, the agreement with the theory is very good. Of note is the convergence of all branches as k goes to zero to a single frequency $\omega\approx 0.0474-0.1144\mathrm{i}$. As pointed

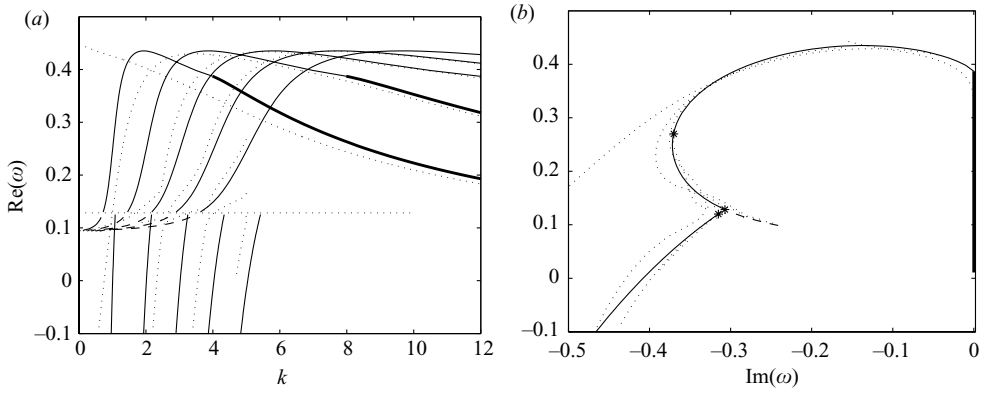

FIGURE 7. Dispersion relation of singular core modes of the Lamb vortex for $m = 2$. (a) Re(ω) versus k. (b) Re(ω) versus Im(ω). The thick solid lines indicate the neutral modes obtained in § 4.1.2. The dotted lines are inviscid numerical results by Fabre *et al.* (2005). The Stokes line structures of the eigenfrequencies indicated by stars in (b) are displayed in figure 8.

out by Sipp & Jacquin (2003), at this frequency, the integration contour is pinched between two critical points. This is clearly visible on the Stokes line network shown in figure 6(b). In our case, this means that a singularity (which cannot be removed) appears in the integral of formula (3.29). The consequence is that the integral becomes divergent, which implies that k has to go to zero. This behaviour is typical; as soon as the integration contour is pinched between two critical points, the wavenumber decreases to zero.

In figure 7 are the results for $m = 2$ together with numerical results by Fabre *et al.* (2005). The results by Fabre *et al.* (2005) have been obtained by an inviscid spectral method. As in Sipp & Jacquin, the integration contour has been deformed in the complex plane. Fabre *et al.* (2005) have also considered viscous effects. They have demonstrated that both $m = 1$ and $m = 2$ damped modes could indeed be obtained by a viscous code with small viscosity, without deforming the integration contour. This confirms that a correct integration contour has been chosen. What is surprising, in figure 7(a), is the discontinuous behaviour of the spatial branches. This discontinuity corresponds to the branch bifurcation shown in figure 7(b) at $\omega \approx 0.1285 - 0.307\mathrm{i}$. This strange behaviour can be traced back to a topological change of the Stokes line structures. The Stokes line network at the crossing-point frequency is shown in figure 8(b). Before and after the bifurcation point, the network has typically the form shown in figures 8(a) and 8(c), respectively. The discontinuous behaviour is therefore associated with a change of turning point. The dashed lines in figure 7 indicate the predictions we would have obtained if we had kept the same turning point in (3.29). Asymptotically, these predictions are not good because the Stokes lines network no longer has the correct topology (as seen in figure 8c). Despite this point, some numerical branches are shown to follow this prediction. For finite wavenumbers, we can imagine that higher-order corrections are no longer negligible and sufficiently modify the Stokes lines to jump from the configuration shown in figure 8(b), to that shown in figure 8(a). For large wavenumbers, i.e. for large n, we are expecting all the branches to follow the solid lines of figures 7.

Larger values of m provide results which are all similar: frequencies are almost real near $\omega \approx m - 2$, and correspond to very large wavenumbers; then, they become strongly damped. In figure 9 the results for $m = 3$ are displayed. A typical Stokes

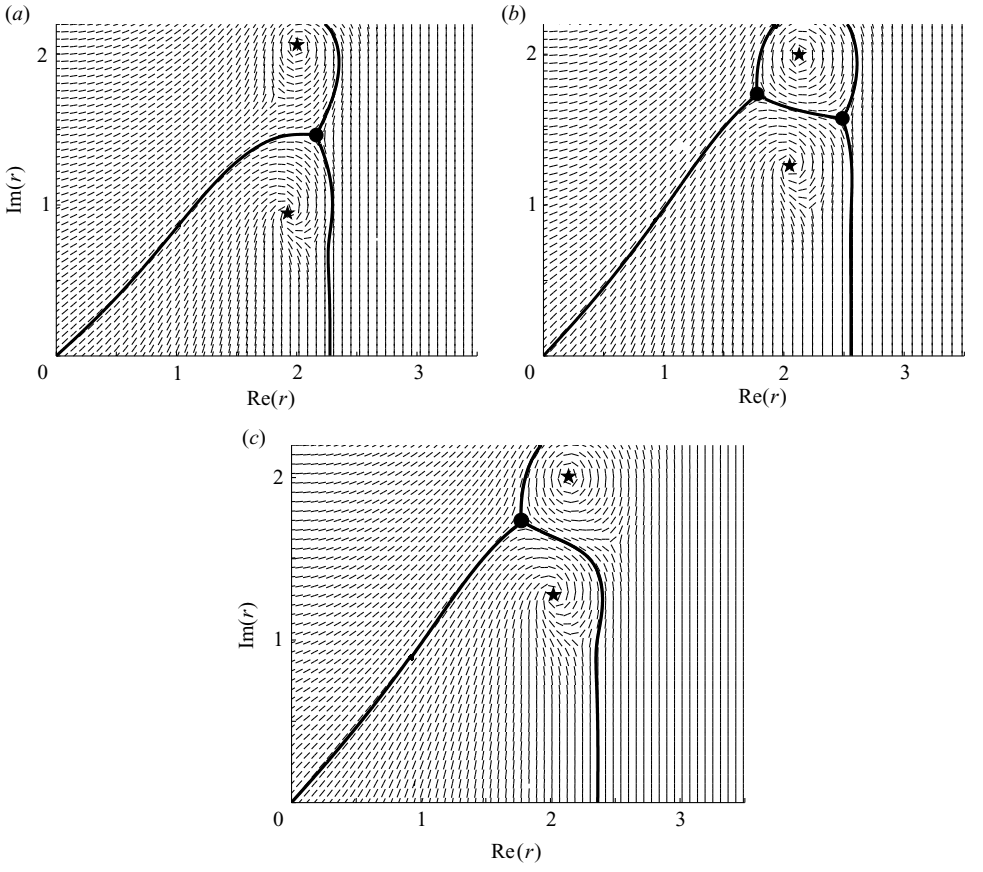

FIGURE 8. Stokes line network for $m=2$ modes of the Lamb vortex. (a) $\omega=0.27-0.37\mathrm{i}$; ($b$) $\omega=0.1285-0.307\mathrm{i}$; ($c$) $\omega=0.12-0.315\mathrm{i}$. See figure 6 for explanation of the symbols.

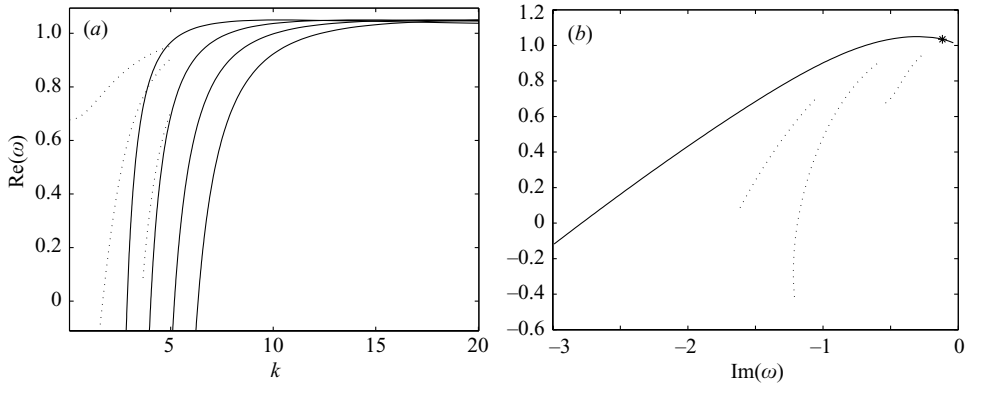

FIGURE 9. Dispersion relation of singular core modes of the Lamb vortex for $m=3$. (a) Re(ω) versus k. (b) Re(ω) versus Im(ω). The dotted lines are inviscid numerical results by Fabre *et al.* (2005). The Stokes line network of the eigenfrequency indicated by a star in (b) is displayed in figure 10.

line network for one of these modes is shown in figure 10. As seen in figure 9, the numerical results do not follow the asymptotic predictions as well as for $m=1$ or $m=2$. This trend was noted above for regular core modes.

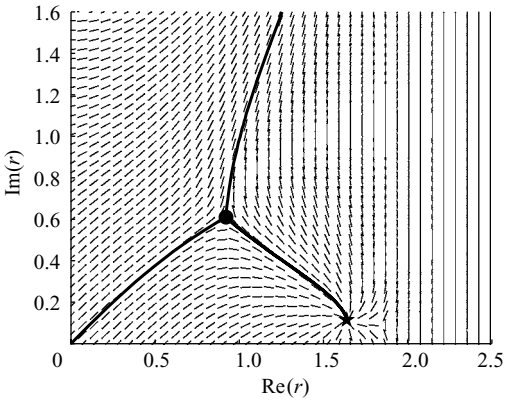

FIGURE 10. Typical Stokes line network for $m \geqslant 3$ modes of the Lamb vortex. Here, $m = 3$ and $\omega = 1.035 - 0.117\mathrm{i}$. See figure 6 for explanation of the symbols.

To close this section on the Lamb vortex, it is important to emphasize the following point. We have been able to identify a few normal modes of the Lamb vortex as core modes. Although we can reasonably think that all the neutral modes have been identified, it is clear that an important number of inviscid damped modes do not enter the category of modes described in this section. In particular, Fabre *et al.* (2005) obtained numerically other families of inviscid damped modes. It is possible to check by looking at their Stokes line structure that these modes are not core modes, but exhibit more complex Stokes line networks.

4.2. *The Gaussian vortex with axial flow (Batchelor vortex)*

In this section, we attempt to account for the effect of an axial flow on the characteristics of the normal modes. The base flow is assumed to be given by (2.3*a*) and (2.3*b*). Only neutral modes will be considered. In particular, we shall not try to follow these modes as they become damped owing to the appearance of a critical point singularity, as was done in the previous section. As already emphasized in § 3, only weak axial flow of order $1/k$ with $k \gg 1$ can *a priori* be considered in the asymptotic framework. However, as the previous asymptotic results have been shown to provide good estimates for small wavenumbers without axial flow, we shall also consider here finite values of the axial flow and finite wavenumbers.

As explained in § 3, the frequency intervals of regular neutral eigenmodes are obtained by looking at the graph of the functions ω^+, ω^- and ω_c. Without axial flow, we have seen that a limited number of behaviours were possible, leading to core modes only. With an axial flow, other behaviours are now possible, but they can only provide ring modes. In figure 11, the functions ω^+, ω^- and ω_c are plotted as a function of the radial coordinate r, for $m = 1$ and $kW_0 = -3$ and for $m = 1$ and $kW_0 = 1.2$. It can be seen in figure 11(*a*), that Hypothesis H2 is here satisfied in the frequency interval (ω_1, ω_2). This means that regular neutral ring modes can be expected in this frequency interval. Note also that, for these parameter values, regular neutral core modes are also expected in the frequency interval $(-4, -2)$.

In the frequency interval (ω_1, ω_2) shown in figure 11(*b*), there exist also ring modes, but they are singular at the critical point which is present for large r. As for singular neutral core modes, we could show that this critical point singularity can be avoided in the complex plane without affecting the dispersion relation which can be calculated for real r. These modes are singular neutral ring modes. We have been able to obtain such modes only for $m = \pm x1$. The regions of the parameter space where ring modes

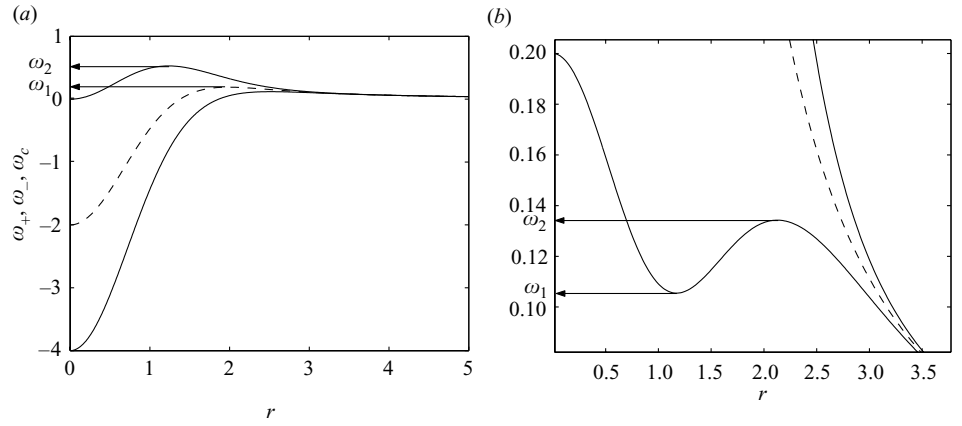

FIGURE 11. The functions $\omega^{\pm}$ (solid lines) and ω_c (dashed line) versus r for the Batchelor vortex and the parameters (*a*) $m=1$, $kW_0=-3$ and (*b*) $m=1$, $kW_0=1.2$. In (*a*), the values ω_1 and ω_2 are the maxima of ω_c and of ω^+, respectively; In (*b*), they are local extrema of ω^-.

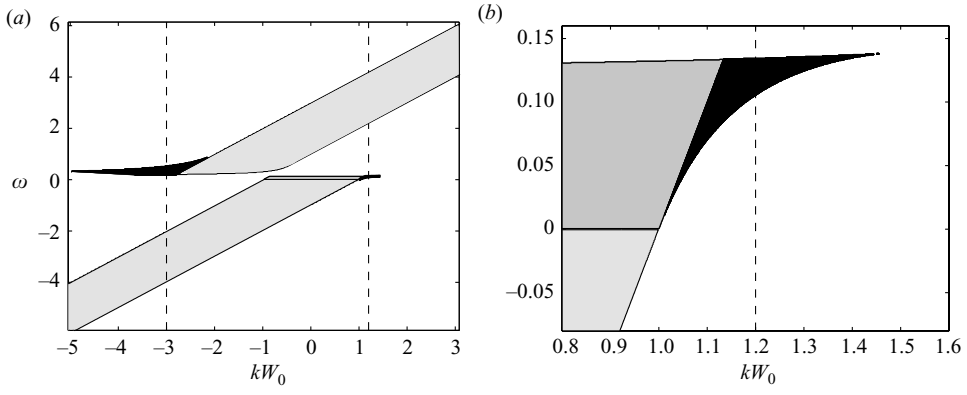

FIGURE 12. Regions of the (ω, kW_0) space where neutral modes of Batchelor vortex are expected for $m=1$. Pale grey, mid grey and black indicate the regular neutral core mode region, the singular neutral core mode region and the neutral ring mode region, respectively. The large black region in (*a*) corresponds to regular neutral ring modes. The small singular neutral ring mode region, almost invisible in (*a*) is enlarged in (*b*). The vertical dashed lines indicated the parameter values for which $\omega^{\pm}$ and ω_c are plotted in figures 11(*a*) and 11(*b*).

are expected are indicated in black in figure 12(*a*) for $m=1$. The region where singular neutral ring modes are expected is very small and limited to the black region shown in figure 12(*b*). In figure 12, the other regions in pale grey and mid grey correspond to regular neutral core modes and singular neutral core modes, respectively. The region corresponding to the conditions (3.9) and (3.10) for the existence of regular neutral modes is merely the union of regular core mode region and regular ring mode region. This means that there is no other regular neutral modes in the white domains of figure 12.

The position of ring mode and core mode regions varies with m. These variations are weak if we plot $\omega - m - kW_0$ instead of ω as demonstrated in figure 13. For negative m, the regions are obtained by the transformation $(\omega, k) \to (-\omega, -k)$. As seen in figure 13, neutral core modes are expected only for frequencies satisfying $-2 < \omega - m - kW_0 < 2$.

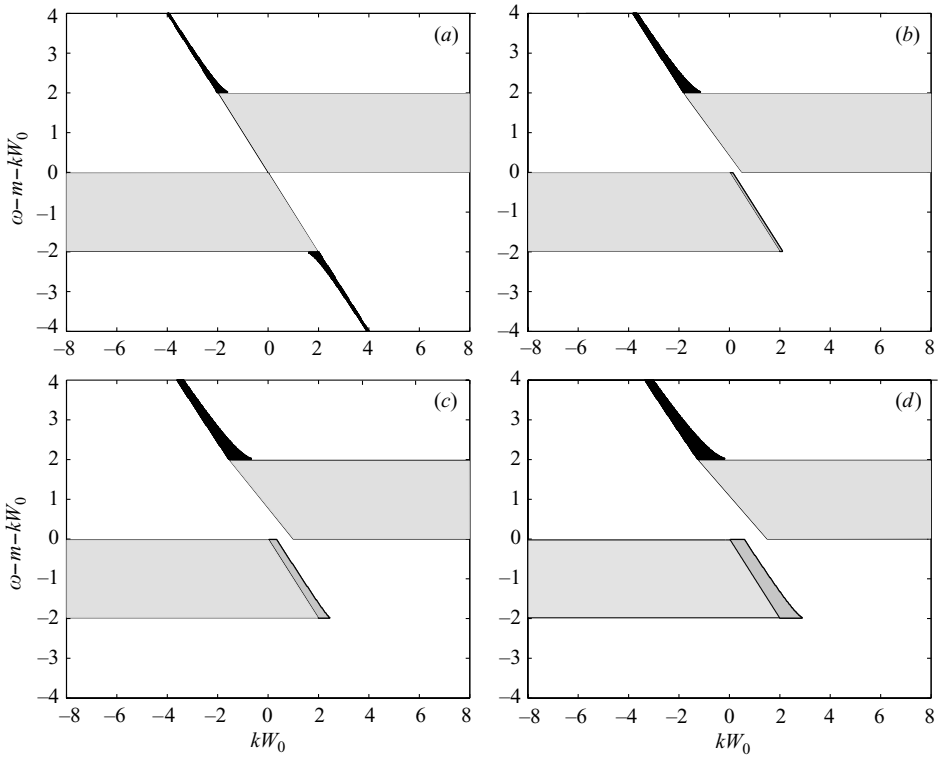

FIGURE 13. Regions of the parameter space where neutral modes of the Batchelor vortex are expected. Pale grey, mid grey and black indicate the regular neutral core mode region, the singular neutral core mode region and the regular neutral ring mode region, respectively. (*a*) $m = 0$; (*b*) $m = 1$; (*c*) $m = 2$; (*d*) $m = 3$. The very small region obtained for $m = 1$ where singular neutral ring modes are expected is not indicated.

By contrast, neutral ring modes are located outside this frequency interval. It is important to stress that (3.9) and (3.10) exactly correspond here to regular core mode and regular ring mode regions. In particular, this implies that there is no regular mode other than those considered here.

Formula (3.29) must be used in both grey regions, while (3.44) must be used in the black regions. As an illustration, the dispersion relation is shown in figure 14 for $m = 1$ and $W_0 = 0.3$, for the first branches. Both numerical results and asymptotic predictions using (3.29) and (3.44) have been plotted. Numerical results have been obtained by a non-viscous shooting method, with a contour deformation procedure for the singular modes. Only neutral modes have been plotted. Numerous singular damped modes, consistent with those obtained in the previous section also exist, but they have not been displayed. Figure 14 demonstrates that (3.29) also works well in the case of a vortex with axial flow. Most of the branches are approximated well, except, as for the case without axial flow, the first branch, which starts from $k = 0$. The predictions for the regular ring modes are also fairly good. Note, however, that there is no singular neutral ring mode for this value of W_0.

Figure 15 shows the radial velocity distribution of two particular eigenmodes as obtained from the asymptotic analysis and from the numerics. A core mode is displayed in figure 15(*a*). The solid curves correspond to the different leading-order

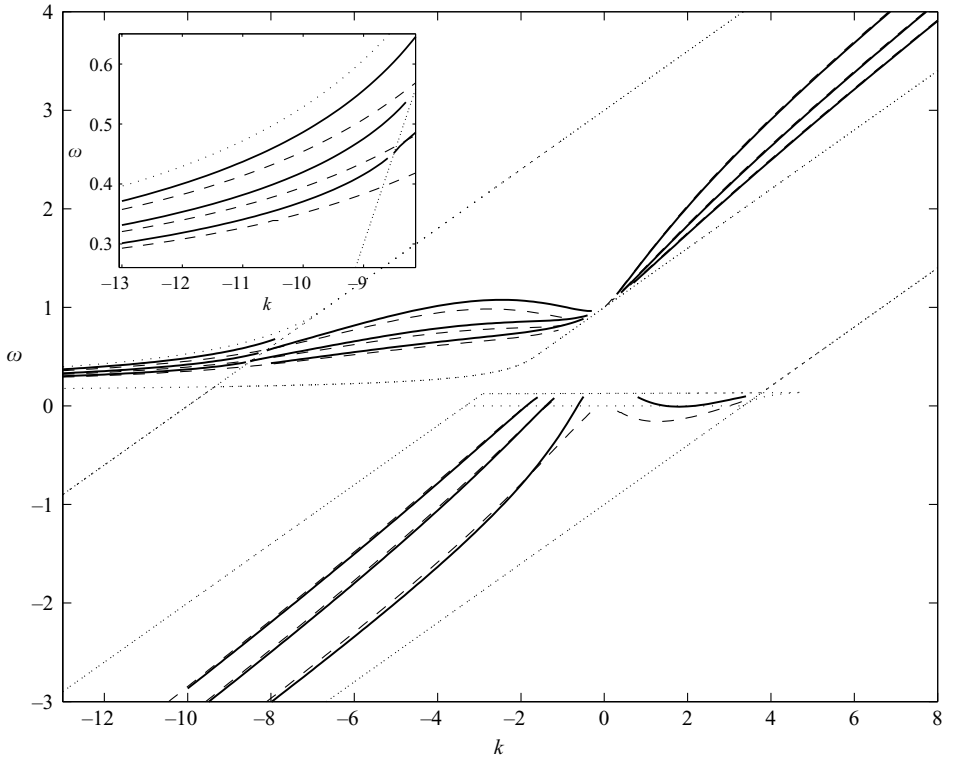

FIGURE 14. Dispersion relation of neutral modes of the Batchelor vortex for $m = 1$ and $W_0 = 0.3$. Solid lines are asymptotic results. Dashed lines are numerical results. Dotted lines are the limits of the regions shown in figure 13. The insert gives a close view of the region associated with regular ring modes.

approximations obtained in § 3.1 near the origin (O), in the core region, near the turning point (T) and in the outer region. The thick part of each solid curve indicates the region where each approximation should apply. As expected, it is in these regions, that the asymptotic results are the closest to the numerical results (dotted curve). A ring mode is shown in figure 15(*b*). In that case, we have used for the solid curves the leading-order approximations obtained in § 3.2 in the outer regions I and II, near each turning point r_1 and r_2 (T1 and T2), and in the ring region. Again, a good agreement of each approximation with the numerics is obtained in the region where the approximation is expected to be valid.

5. Conclusion

In this paper, an asymptotic description of the normal modes in a stable vortex has been proposed. It is based on a large axial wavenumber WKBJ analysis. A considerable effort has been made to connect the properties of the neutral modes to the characteristics of the base flow. In particular, we have shown how the analysis of a few quantities which are the epicyclic frequencies $\omega^{\pm}(r)$, and the critical frequency $\omega_c(r)$ defined in (3.7) and (3.8), respectively, permits the regions of existence of neutral modes to be located in the parameter space. Two types of neutral normal mode have been considered, which are either confined in the vortex core (core modes) or in a ring (ring modes). General dispersion relations have been derived for both cases. In the

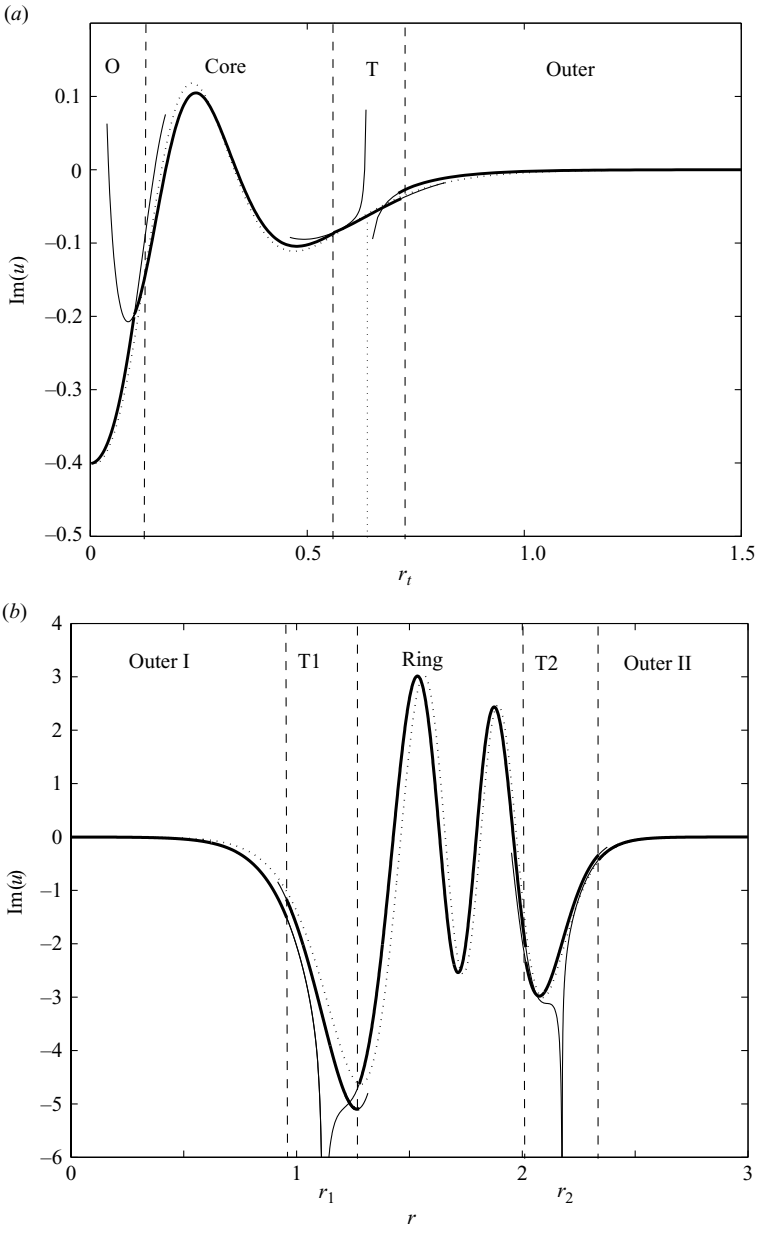

FIGURE 15. Radial velocity profiles of eigenmodes of the Batchelor vortex for $W_0 = 0.3$. Dotted curve: numerical results. Solid curves: asymptotical approximations. The different regions of the asymptotical analysis are also indicated. The solid curve is thicker in the region where the approximation is expected to be valid. (*a*) Regular core mode ($m = 1$, $k = 8$, $\omega \approx 3.91$); (*b*) Regular ring mode ($m = 1$, $k = -13$, $\omega \approx 0.27$).

WKBJ terminology, core modes correspond to oscillating modes between the origin and a turning point, while ring modes are oscillating modes between two distant turning points. The asymptotic dispersion relations have been applied to a Gaussian vortex with and without axial flow. For the Gaussian vortex without axial flow (Lamb vortex), neutral modes have been shown to be core modes only. Their asymptotic

dispersion relation has been found to be in very good agreement with numerical results, even for small values of the wavenumber. For the Gaussian vortex with axial flow (Batchelor vortex), neutral modes have been shown to be either core modes or ring modes. A comparison with the numerics has been carried out in a single case, and a good agreement has also been observed, for both core modes and ring modes. The spatial structure of the eigenmodes has also been shown to be reproduced well.

The influence of critical point singularities has been analysed in detail. We have shown that core modes can remain neutral at leading order, even if they possess a critical point singularity. Such 'singular neutral core modes' have been exhibited for $m=1$ and $m=2$ in the case without axial flow. They have also been shown to exist in the presence of axial flow. The critical point singularity damps the normal modes when it enters the core region. We have shown that the associated complex eigenfrequencies can still be computed with the same relation applied in the complex plane if the critical point singularities are correctly avoided in the complex plane following Lin's rule. This rule guarantees that the vanishing viscosity limit of genuine viscous eigenfrequencies is considered. However, a fine monitoring of the evolution of turning points and critical points must be performed to track the different branches. This procedure has been carried out for two families of modes for the Lamb vortex ($m=1$ and $m=2$). The frequencies of damped core modes which have been obtained in this way, have been compared favourably with numerical simulations by Sipp & Jacquin (2003) and Fabre *et al.* (2005). We have been able to provide an explanation to the peculiar behaviour of the branches for $m=2$: two different turning points have been shown to intervene in the eigenvalue relation.

For the applications, it is important to emphasize that the present theory permits us to obtain information on neutral modes by a very simple procedure. We therefore expect our asymptotic results to be valuable for describing instabilities, such as the elliptic instability, which result from the interaction of neutral modes. As reviewed by Kerswell (2002), the elliptic instability is due to the resonance of two normal modes with the underlying strain field responsible for the elliptic deformation of the vortex. When the strain field is stationary, two neutral modes resonate if their frequencies and axial wavenumbers are identical, and their azimuthal wavenumbers differ by 2 (see e.g. Kerswell 2002). The present analysis allows to locate easily the regions of the parameter space where two neutral normal modes of azimuthal wavenumbers $m-1$ and $m+1$ can possibly resonate; we just have to find the intersection of the regions where the two neutral modes exist. For the Batchelor vortex studied in § 4.2, this procedure leads to the results displayed in figure 16. In each of these regions, resonance is *a priori* possible. Moreover, from the nature of the mode in each region, we have the following information: resonance is possible only between regular neutral core modes and singular neutral core modes. In particular, this implies that ring modes cannot be excited resonantly by the elliptical instability. The fine analysis of the resonance conditions in each region and its dependence with respect to W_0 is an important issue which could have applications in the aeronautical context, where the elliptical instability in a vortex with axial flow is known to be present. This will be the subject of a future study.

While we have focused on stable vortices, it is worth emphasizing that the same analysis could also be useful for describing unstable modes in other types of vortex. For instance, the axisymmetric unstable modes associated with the centrifugal instability can be captured by our analysis. These modes are stationary and localized in the radial region where the Rayleigh discriminant $\Upsilon(r)=2\Omega(r)\zeta(r)$ is negative (e.g. Rossi 2000). Bayly (1988) demonstrated that a large k-asymptotic analysis could be

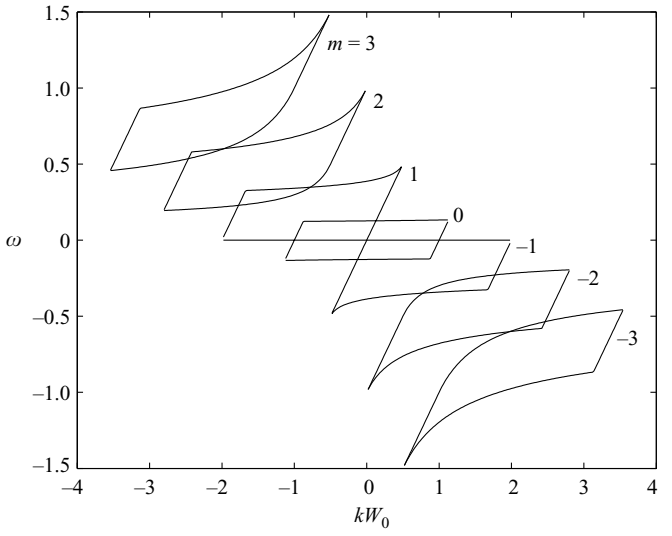

FIGURE 16. Region in the (ω, kW_0) space of possible resonance of two neutral normal modes of azimuthal wavenumbers $m-1$ and $m+1$ for various m for the Batchelor vortex.

possible to describe these modes. With our terminology, these modes would be ring modes localized between two turning points satisfying $\Delta = 0$, i.e. $\Phi(r) = -\mathrm{Im}(\omega)$. The most unstable modes would correspond to the configuration where the two turning points are close to the minimum of Υ. We refer to Bayly (1988) and Rossi (2000) for details. Gallaire & Billant (2003) have shown that the same analysis could also be used to extend the Rayleigh instability criterion to non-axisymmetric modes.

This work has benefited from discussions with D. Fabre, A. Antkowiak and F. Gallaire. We would also like to thank D. Sipp and D. Fabre for having provided the numerical data plotted in figures 5, 7 and 9. Thanks also to Kris Ryan for his careful reading of the manuscript.

REFERENCES

ABRAMOWITZ, M. & STEGUN, I. A. 1965 *Handbook of Mathematical Functions*. Dover.

ARENDT, S., FRITTS, D. C. & ANDREASSEN, O. 1997 The initial value problem for Kelvin vortex waves. *J. Fluid Mech.* **344**, 181–212.

ASH, R. L. & KHORRAMI, M. R. 1995 Vortex stability. In *Fluid Vortices* (ed. S. I. Green), chap. 8, pp. 317–372. Kluwer.

BAYLY, B. J. 1988 Three-dimensional centrifugal-type instabilities in inviscid two-dimensional flows. *Phys. Fluids* **31**, 56–64.

BENDER, C. M. & ORSZAG, S. A. 1978 *Advanced Mathematical Methods for Scientists and Engineers*. McGraw–Hill.

DRAZIN, P. G. & REID, W. H. 1981 *Hydrodynamic Stability*. Cambridge University Press.

FABRE, D. 2002 Instabilités et instationnarités dans les tourbillons: application aux sillages d'avions. PhD thesis, ONERA/Université Paris VI.

FABRE, D., SIPP, D. & JACQUIN, L. 2005 The Kelvin waves and the singular modes of the Lamb–Oseen vortex. *J. Fluid Mech.* (in press).

FEDORYUK, M. V. 1993 *Asymptotic Analysis*. Springer.

GALLAIRE, F. & BILLANT, P. 2003 Generalized Rayleigh criterion for non-axisymmetric centrifugal instabilities. *Bull. Am. Phys. Soc.* **48**(10), 66.

GREENSPAN, H. P. 1968 *The Theory of Rotating Fluids*. Cambridge University Press.

Kerswell, R. R. 2002 Elliptical instability. *Annu. Rev. Fluid Mech.* **34**, 83–113.

Landau, L. & Lifchitz, E. 1966 *Mécanique Quantique, Théorie non Relatiste*. Éditions MIR.

Le Dizès, S. 2004 Viscous critical-layer analysis of vortex normal modes. *Stud. Appl. Maths* **112**, 315–332.

Lin, C. C. 1955 *The Theory of Hydrodynamics Stability*. Cambridge University Press.

Olver, F. W. J. 1997 *Asymptotics and Special Functions*. A. K. Peters.

Rossi, M. 2000 Of vortices and vortical layers: an overview. In *Vortex Structure and Dynamics* (ed. A. Maurel & P. Petitjeans), pp. 40–123. Springer.

Saffman, P. G. 1992 *Vortex Dynamics*. Cambridge University Press.

Sipp, D. & Jacquin, L. 2003 Widnall instabilities in vortex pairs. *Phys. Fluids* **15**, 1861–1874.

Stewartson, K. & Brown, S. 1985 Near-neutral-centre-modes as inviscid perturbations to a trailing line vortex. *J. Fluid Mech.* **156**, 387–399.

Stewartson, K. & Leibovich, S. 1987 On the stability of a columnar vortex to disturbances with large azimuthal wavenumbers: the upper neutral points. *J. Fluid Mech.* **178**, 549–566.